Atoms in an amplitude-modulated standing wave - dynamics and pathways to quantum chaos

2000 J. Opt. B: Quantum Semiclass. Opt. 2 659

(http://iopscience.iop.org/1464-4266/2/5/314)

J. Opt. B: Quantum Semiclass. Opt. **2** (2000) 659–667. Printed in the UK PII: S1464-4266(00)11627-1

Atoms in an amplitude-modulated standing wave—dynamics and pathways to quantum chaos

W K Hensinger, A G Truscott, B Upcroft, N R Heckenberg and H Rubinsztein-Dunlop

Centre for Laser Science, Department of Physics, The University of Queensland, Brisbane, Queensland 4072, Australia

Received 4 February 2000, in final form 7 June 2000

Abstract. Cold rubidium atoms are subjected to an amplitude-modulated far-detuned standing wave of light to form a quantum-driven pendulum. Here we discuss the dynamics of these atoms. Phase space resonances and chaotic transients of the system exhibit dynamics which can be useful in many atom optics applications as they can be utilized as means for phase space state preparation. We explain the occurrence of distinct peaks in the atomic momentum distribution, analyse them in detail and give evidence for the importance of the system for quantum chaos and decoherence studies.

Keywords: Atom optics, decoherence, quantum chaos, atom cooling and trapping

1. Introduction

Cold atoms have been used in a variety of experiments. Here we report on the dynamics of cold atoms exposed to a modulated standing light wave. There are many different effects that can occur when atoms are subjected to a standing wave of light. A standing wave can be used to diffract atoms to act as a coherent beam splitter. This interaction is similar to Bragg diffraction of light by a crystal [1] and is used for interferometry applications. Anderson *et al* have used cold atoms in a standing wave to demonstrate an effect similar to the AC Josephson effect [2]. In this experiment the interference of atoms tunnelling through light potentials was observed. To observe a Wannier–Stark ladder, Raizen's group has subjected cold atoms to a phase-modulated accelerating standing wave [3]. In yet another experiment a far-detuned standing wave has been used to focus an atomic beam. The atoms traversed the standing wave field and each node acted as an individual lens, the entire standing wave being equivalent to an array of lenses. Using this principle permanent nanostructures were created with Cr atoms [4].

An optical standing wave can be used to manipulate atoms and prepare them to have a certain momentum (as we will show later in this paper) for various atom optics applications. Standing wave experiments can also be used to study one of the frontiers of physics, the field of 'quantum chaos' and decoherence. Quantum chaos deals with quantum behaviour in classically chaotic systems. It is the desire to understand the quantum mechanical origin of the observed chaos which drives this area of research. Chaos can be interpreted as the rapid divergence of arbitrarily close points in phase space. This concept is not really compatible with structure being smoothed away on small scales of phase space volume ($<\hbar$), due to the Heisenberg uncertainty principle [5,6]. In fact, the quantum classical correspondence for dynamical systems is still unclear and a subject of discussion. Decoherence plays an integral role.

Graham *et al* [7] proposed to use cold atoms to study quantum chaos. Cold atoms in a standing light wave are an ideal system to study quantum and classical dynamics and the effects of decoherence. The dynamics can be carefully controlled using a wide array of possible optical potentials. Decoherence can be introduced in two ways, either by the addition of specific noise to the modulation of the optical standing wave, or by changing the detuning of the standing wave, increasing the amount of spontaneous emission and therefore producing random recoil kicks on the atoms.

Moore *et al* [8] and Ammann *et al* [9] have used cold atoms to simulate the quantum delta-kicked rotor (Q-DKR). Here the standing wave is periodically turned on and off and the atomic momentum distribution is measured as a function of the number of kicks. The first experimental observation of dynamical localization (quantum suppression of chaotic diffusion) in cold atoms was reported by Raizen's group [10]. The trajectories of atoms can interfere destructively, hindering the atomic diffusion. Dynamical localization can be observed by measuring the kinetic energy of atoms as a function of the number of kicks. While classically, one would expect to observe linear growth proportional to the classical diffusion constant, it is observed in the experiment that, after the quantum break time, the measured energy stops growing, in agreement with the quantum prediction. In this system decoherence

1464-4266/00/050659+09$30.00

was applied in a controlled way using amplitude noise and near-resonant optical molasses [9, 11]. It was found that both factors led to the destruction of dynamical localization. Therefore decoherence might be considered as the link between the classical and quantum worlds, validating the quantum/classical correspondence principle.

To gain a better insight into quantum chaos, it is important to design experiments where one can vary and control the scaled Planck's constant of the system. If this is possible, then the degree of divergence between quantum and classical physics can be analysed for different values of the scaled Planck's constant. Furthermore, it is possible to test whether the introduction of decoherence into a system is equivalent to the limit of Planck's constant going to zero. This goal may be achieved when using the system of the quantum-driven pendulum (QDP). It corresponds to the dynamics of atoms in an amplitude-modulated standing wave. The scaled Planck's constant $\bar{k}$ for this system is inversely proportional to the modulation frequency of the standing wave, which can be varied to investigate both classical and quantum regimes. Our group has already seen evidence for the occurrence of quantum effects in this system for large values of $\bar{k}$ [12]. In this present paper we will present some of our results for the QDP which are related to the area of quantum chaos. We will discuss the origin of distinct peaks in the momentum distribution and analyse some of their properties. The QDP has a mixed phase space consisting of regions of regular motion (resonances) which are bounded by Kolmogorov, Arnold and Moser (KAM) surfaces [13] surrounded by a sea of chaos. The resonances are a distinct feature of the atomic momentum distribution. To date, we know of two kinds of quantum effects for this system. Firstly, the velocity of the resonances predicted in quantum and classical models differs significantly for values of large $\bar{k}$. A velocity shift was predicted theoretically by Milburn *et al* in the theory of quantum slow motion [14].

The second quantum effect which has been discussed is quantum phase space tunnelling. As predicted by Dyrting *et al* [15, 16] atoms can coherently tunnel from one region of regular motion to another. To do this, atoms have to cross KAM surfaces, which is forbidden classically. The tunnelling effect can be pictured as atoms tunnelling from one kind of oscillatory motion to another oscillatory motion which is 180° out of phase. This means that atoms do not only tunnel in position but also in momentum. Our aim is to construct an experimental procedure to study this phenomenon. Once phase space tunnelling is implemented the system is an ideal testbed for studies of decoherence. We will discuss here some possible methods for observation of the tunnelling. We will also present some new results on the dynamics of phase space resonances.

2. Description of the experimental setup

In order to study the effects of a standing wave on cold atoms a source of such atoms is needed. In our experiments rubidium atoms are cooled down to around 8 μK (corresponding to a $1/e$ momentum spread of 13 recoil momenta) in a standard magneto-optic trap (MOT) [17]. The specifications of the MOT are as follows. The pressure in the vacuum chamber is around 10^{-9} Torr. The magnetic field coils produce a magnetic field gradient of 10^{-1} T m^{-1} in an anti-Helmholtz configuration. Zeroing of the Earth's magnetic field is achieved using the Hanle effect [18]. When applying a magnetic field the magnitude of absorption of the laser beams changes slightly when the laser is at resonance with the atomic vapour. This can be used to zero the magnetic field with high precision. An injection locking scheme is utilized to decrease the linewidth of the trapping diode laser down to 100 kHz, while allowing all the power of the laser to be used in the trapping experiment. Around 10^6 rubidium atoms are polarization-gradient cooled for 10 ms. Then the MOT is turned off but the repumping beam is left on so that the atoms accumulate in the $F = 3$ ground state. We wait for 500 μs to allow for effective repumping. The standing wave is turned on for a precise duration and is intensity modulated using an AOM as described below. After the standing wave is switched off, the atoms undergo a period of ballistic expansion (between 3–20 ms). Following this, an image of the cloud is taken using a freezing molasses technique [8, 19]. In this technique the optical molasses is turned on again, with the magnetic field still turned off. As a result of this the atomic distribution is frozen at its current position and the fluorescence resulting from the 'frozen' atoms is viewed with a 16-bit charged coupled device (CCD) camera. The CCD array of the camera is cooled, leading to a quantum efficiency of around 80% and a RMS read noise of 6.7 electrons. The experiment is repeated multiple times with different ballistic expansion times to allow a statistical measurement of the velocity of the atoms with high precision.

The experimental setup is shown in figure 1. The standing wave is produced using a frequency-stabilized titanium sapphire laser (Ti–S). It produces up to 2 W of light at 780 nm with a linewidth of 1 MHz. To reduce the intensity noise, polarization noise and pointing instability to less than 1% we have implemented the following technique. The Ti–S beam is first passed through an 80 MHz acousto-optic modulator (denoted by AOM_1 in figure 1) and the zeroth order is fed into a polarization-preserving single-mode optical fibre. Part of the output beam from the fibre is leaked through a mirror and a polarizer to a photodetector, which gives an electronic feedback signal to the AOM_1 on the other end of the fibre to compensate for fluctuations. In our experiments we modulate the intensity of the optical standing wave. AOM_2 (as seen in figure 1) modulates this beam and produces an intensity modulation of the form $I_0(1 + 2\varepsilon \cos \omega_m t)$ where ε is the depth of modulation, ω_m is the modulation angular frequency and I_0 the unmodulated intensity. After the light has passed through AOM_2 and the vacuum chamber, we regularly monitor the beam quality in the far field, utilizing a lens to expand the beam to ensure that a regular Gaussian profile is maintained. To test the spectral purity of our modulated standing wave the modulated light wave was observed on a fast photodetector and subsequent Fourier analysis of this signal indicated a spectral impurity of about one part in a thousand. The light after AOM_2 was collimated to a $1/e$ width of 3.25 mm. The beam passes through the vacuum chamber and through the atomic cloud and is retroreflected to form the one-dimensional periodic optical potential. There are several procedures to align the

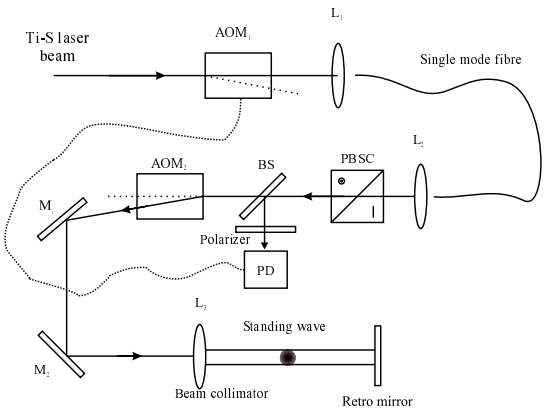

Figure 1. Schematic diagram of the experimental setup. L_1, L_2 are lenses used to couple the laser beam in and out of the optical fibre which is utilized to optimize the pointing stability and to improve the quality of the laser beam. AOM_1 is used for stabilization of the light intensity. AOM_2 produces the intensity modulation which is needed to produce an amplitude-modulated standing wave.

beam so that the beam is centred on the cloud. In one method the light frequency is tuned close to the spectral resonance of the trapped atoms. The beam is then moved until it blows the trapped atoms out of the centre of the trap, which can be observed on a CCD camera. This is good for rough alignment. The light is then further detuned and the alignment is improved by ensuring that all the atoms are blown out of the trap again. Subsequent iterations of this procedure lead to a precise alignment of the incoming beam. The retroreflection is aligned using an aperture located far away from the retro mirror just before the output of the single-mode polarization-preserving fibre. A beam splitter, located right between the aperture and fibre output reflects light only if the retroreflection passes through the aperture. The alignment of the retroreflection was measured to be good to approximately 0.02°. We have measured the variation of the scaled well depth κ over the extent of the atomic cloud to be approximately 2%. The final maximum irradiance of the standing wave in the region of the atomic cloud was 12 ± 0.5 W cm^{-2}. A telescope before AOM_2 is used to decrease the beam diameter and consequently increase the efficiency of the AOM. Using another telescope after AOM_2 the beam diameter can be controlled and the beam is carefully collimated. The whole experiment is computer controlled using the LabVIEW programming environment and a GPIB interface.

3. The QDP

As mentioned before, the QDP corresponds to atoms in an amplitude-modulated standing wave. A thorough theoretical treatment of the system can be found in Hensinger *et al* [12]. The dynamics of the atoms along the axis of the standing wave can be calculated using the master equation for the system. In the interaction picture this is given by

$$\dot{\rho} = -\frac{\mathrm{i}}{\hbar}[H, \rho] + \Gamma \mathcal{L}_1 \rho. \tag{1}$$

Here H is the Hamiltonian for the centre-of-mass and internal state of the atom. The superoperator $\mathcal{L}_1$ describes the incoherent evolution due to the coupling to the vacuum field modes at a rate Γ. To calculate the dynamics of the atoms the excited state of the atom is adiabatically eliminated [12]. This is justified if the detuning of the standing wave δ is much greater than the maximum of the Rabi frequency $\Omega(x, t)$. Adiabatic elimination leads to an effective Hamiltonian for the centre-of-mass motion given by [20]

$$H = \frac{p_x^2}{2m} + \frac{\hbar\Omega_{\mathrm{eff}}}{4}(1 + 2\varepsilon\cos\omega_m t)\sin^2(kx) \tag{2}$$

where the effective Rabi frequency is $\Omega_{\mathrm{eff}} = \Omega^2/\delta$, $\Omega = \Gamma\sqrt{I/I_{\mathrm{sat}}}$ is the resonant Rabi frequency, ε is the depth of modulation, ω_m is the modulation angular frequency, Γ is the inverse spontaneous lifetime, t is the time, p_x the momentum component of the atom along the standing wave and m the mass of a Rb atom. Here I is the spatial mean of the intensity of the unmodulated standing wave (which is half of the peak intensity so $\Omega = \Gamma\sqrt{I_{\mathrm{peak}}/2I_{\mathrm{sat}}}$) and I_{sat} is the saturation intensity. Using scaled variables [8] the Hamiltonian is given by

$$\mathcal{H} = p^2/2 + 2\kappa(1 + 2\varepsilon\cos\tau)\sin^2(q/2) \tag{3}$$

where $\mathcal{H} = (4k^2/m\omega_m^2)H$, $q = 2kx$, $p = (2k/m\omega_m)p_x$ and k is the wavenumber. The driving amplitude is given by

$$\kappa = \frac{\hbar k^2 \Omega_{\mathrm{eff}}}{2\omega_m^2 m}. \tag{4}$$

$\tau = t\omega_m$ is the scaled time variable. This system can be classified as a driven pendulum, because the Hamiltonian is equivalent to that of a driven pendulum [15].

To calculate the dynamics of the atoms we are using two different methods for our quantum simulations. The full master equation treatment is carried out using the momentum state basis. Spontaneous emission following the absorption of a photon from the standing wave enables a transfer of momentum of any amount between $-2\hbar k$ and $+2\hbar k$ to the atom. This means that an exact simulation of the master equation would require a dense set of momentum states. On the other hand, the initial conditions from the experimental setup have a momentum spread of the order of $7\hbar k$, which means that features of the order of $\hbar k$ are not resolvable. It therefore makes sense to approximate the continuous momentum transfer due to spontaneous emission by discrete momentum transfer in units of $\hbar k$, in order to take advantage of the symmetry of the Hamiltonian. This leads to a momentum state basis given by $|p_0 + \hbar k n\rangle$ (where p_0 is an arbitrary momentum and n is an integer). The initial-state matrix $\langle n|\rho(0)|n\rangle$ is found by assuming a Gaussian initial momentum distribution of $1/e$ half-width of $6.5\hbar k$ which forms the diagonal elements of $\rho(0)$. The second method we use to produce our simulations is the theory of quantum trajectories [21]. It was shown [22] that it is possible to simulate incoherent transitions using Monte Carlo methods, so this was done to obtain our second kind of quantum mechanical simulation. A stochastic Schrödinger equation developed for atom optics by Dum *et al* [23] and Mølmer *et al* [24] is used to include incoherent transitions [12]. Roughly speaking, the stochastic Schrödinger equation includes the smooth evolution of the initial wavepacket with the Hamiltonian (3), together with point processes

(incoherent transitions) which are included with a Monte Carlo method. The advantage of this approximation is that it has a clear classical analogue.

For our classical simulations we use Hamilton's equations to calculate the dynamics of the system. To obtain a realistic model, incoherent transitions have been included in the classical simulation. This can be done analogously to the quantum trajectory simulation using a Monte Carlo simulation.

The scaled Planck's constant, which is the commutator of scaled position and momentum coordinates, can be rewritten as

$$\bar{k} = \frac{4\hbar k^2}{\omega_m m} = 4\hbar \frac{4\pi^2}{\lambda^2 \omega_m} = 4\hbar\pi^2 \left(\frac{1}{\frac{\lambda}{2}(\frac{\lambda}{2T} m)} \right) = \frac{4\hbar\pi^2}{2\pi I_0} = \frac{h}{I_0} \tag{5}$$

where T is the modulation period, $\hbar$ is Planck's constant, λ is the wavelength and I_0 is the action of a free particle over the distance $\lambda/2$ in the time T. Our one-dimensional system can be described in the corresponding two-dimensional phase space which is spanned by momentum and position coordinates. The action of the system, multiplied by 2π, is given by the area in phase space, which is encircled by the trajectory of a particle. $\bar{k}$ can be interpreted as the ratio of Planck's constant to the action of a free particle in the system described. Thus $\bar{k}$ will indicate in which regime the experiment is carried out [5]. Therefore we know there is some minimum order of magnitude of $\bar{k}$ which must be exceeded before we expect to see differences between quantum and classical dynamics on a given timescale. We have seen in our simulations that significant differences between classical and quantum mechanical simulations arise with values of $\bar{k} \gtrsim 0.1$. To introduce some kind of rough classification we characterize values of $\bar{k} \gtrsim 0.1$ as the quantum regime while we classify the classical regime with values of $\bar{k} \lesssim 0.1$.

The main source of decoherence introduced into the system results from incoherent transitions (e.g. spontaneous emission). This can be controlled by changing the detuning of the modulated standing wave.

To understand the dynamics of the QDP it is convenient to use Poincaré sections with the stroboscopic period equal to the modulation period. Figure 2 shows Poincaré sections for the QDP. One can see islands of regular motion in a sea of chaos. While the islands correspond to atoms oscillating with a certain phase relative to each other inside the well, the random dots correspond to atoms bouncing chaotically inside the well. The size and the position of the islands of regular motion depend very strongly on the system parameters. Using scaled variables the phase space depends only on κ and ϵ. The sea of chaos is bounded by the region of regular unbound motion, corresponding to atoms which have enough kinetic energy to move from one well to the next. The ratio of kinetic energy of the atoms having $1/e$ velocity to the potential energy of the well is of the order of 10^{-2} (detuning $\delta = 4.3$ GHz). To give an overview of the dynamics of the QDP, figure 2 shows the phase space for ϵ constant and κ varied in parts (*a*)–(*c*), as well as κ constant and ϵ varied in parts (*d*)–(*f*). It can be seen that the position of the resonances is a function of κ. Furthermore, one can see that the size of the resonances is dependent on the modulation amplitude ϵ. While the second-order resonances of interest are obvious above and below the central island of stability, one can also see the emergence of period 1 resonances just below the separatrix, especially for higher values of the modulation amplitude ϵ.

4. Experimental dynamics of the QDP

4.1. Dynamical properties of the phase space resonances

Figure 3 shows the optical potential after fractions of the modulation period. To illustrate the concept of phase space resonances and the loading and observation of the resonances (period 2), the optical potential is shown for four phases of the modulation period. Atoms are randomly spaced inside the potential well when the potential is turned on. For our current experimental setup the resonances are loaded when they are located on the position axis, which is determined by the start phase of the modulation of the standing wave. Let us consider approximately stationary atoms (along the standing wave). Only atoms which have a certain position inside the well can be loaded into the resonances. These atoms oscillate inside the well in regular motion (atom groups 1 and 2 correspond to atoms contained in the resonance). After one modulation period atom groups 1 and 2 have exchanged their positions. From dynamical theory and the Poincaré sections it follows that only atoms whose initial position inside the potential well corresponds to an oscillation frequency equal to half of the modulation frequency are contained in a resonance. All the other atoms whose initial position corresponds to different oscillation frequencies will bounce chaotically inside the potential well and will form the chaotic background of atoms in the momentum distribution observed in the experiment. It is experimentally impossible to resolve structure inside one of the potential wells. Therefore, to observe the resonances the standing wave is turned off after $N + \frac{1}{2}$ periods of the modulation (N is an integer). At this point in time atom groups 1 and 2 will have maximum velocity in opposite directions. After a ballistic expansion time of typically 10–20 ms the atom groups 1 and 2 can be spatially resolved and identified as phase space resonances. The resonances of the QDP can thus be observed as peaks in the momentum distribution. Spatial distributions of the atoms can be taken for different ballistic expansion times to effectively calibrate the position axis into a momentum scale. Figure 4 shows the spatial distributions obtained after a 10 ms ballistic expansion interval. The upper distribution results when no interaction potential is applied. The lower distribution shows the resonant structure that results when the atoms interact with 7.5 cycles of a modulated standing wave (using a modulation frequency $\omega_m/(2\pi) = 500$ kHz and a modulation parameter $\epsilon = 0.13$). The actual velocities can be determined more precisely from measurements of the peak positions as a function of ballistic expansion time.

Although resonances of the QDP occur for a variety of parameters, due to nonlinear dynamics the size of the resonances varies strongly. In our experiments we have found a value of κ which maximizes the number of atoms contained in the resonances. We first selected one modulation

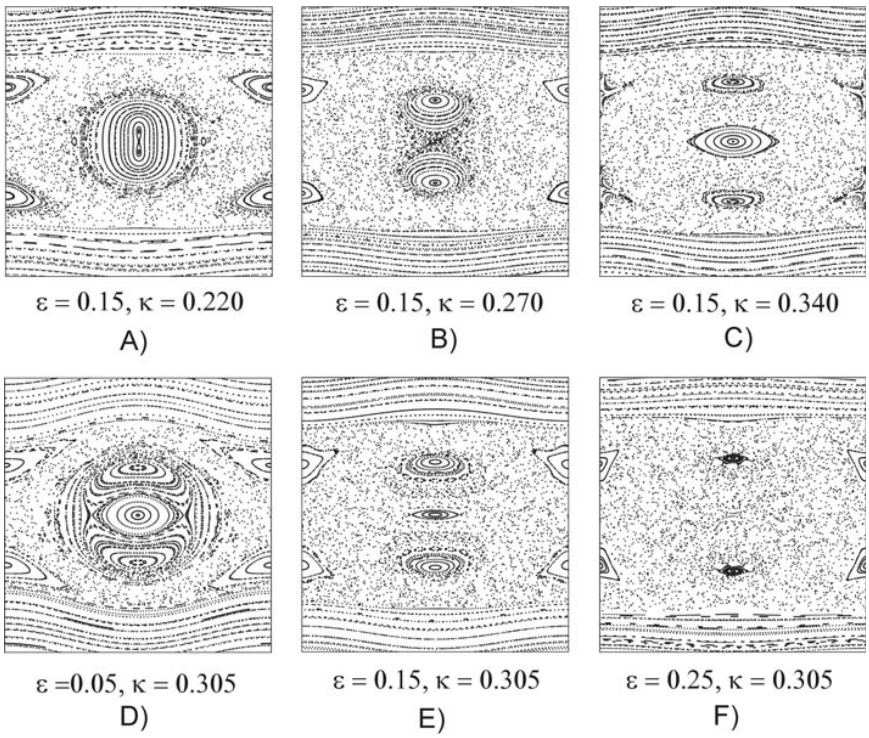

Figure 2. Poincaré sections for the QDP. The x-axis of this figure is the scaled position variable q and the y-axis of the plots is the scaled momentum p. In parts (a)–(c) the modulation amplitude ϵ is held constant and the driving amplitude κ is varied while in parts (d)–(f) κ is held constant and ϵ is varied. The size and position of the resonances strongly depends on the system parameters ϵ and κ. The small period-1 resonances positioned on the side of the Poincaré section just below the region of unbound regular motion do not rotate and therefore never cross the position axis. This means that they will not be loaded in the experiment and thus cannot be seen in the atomic momentum distribution.

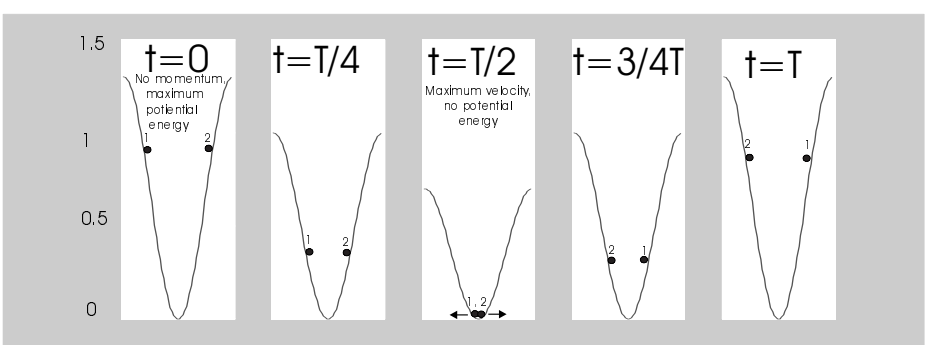

Figure 3. Potential after fractions of the modulation period. Groups 1 and 2 correspond to atoms contained in upper and lower resonances (see Poincaré section). The position of the these two groups, as well as the potential, is shown for four phases of the modulation. Atoms which start in the resonances start with zero velocity at the top of the potential. After half of the modulation period they have reached the bottom of the well and have reached their maximum velocity.

frequency and then adjusted the detuning δ for maximum height of the resonance peaks in the atomic momentum distributions. During the procedure we kept the light intensity constant. Figure 5 shows the position of the resonances in terms of the system parameters ω_m and δ. We know that the driving amplitude κ is inversely proportional to the detuning δ and the square of the modulation frequency ω_m ($\kappa \sim (\omega_m^2 \delta)^{-1}$). Therefore, if there is a linear relationship between $1/\omega_m^2$ and the detuning δ one can conclude that κ is a constant, being proportional to the slope of the graph. We could load up to 50% of all atoms into the resonances using optimum values for κ and ε.

We have found that the resonances are maximized for the scaled driving amplitude $\kappa = 0.4 \pm 0.1$ ($\varepsilon = 0.13$). Nonlinear dynamics theory tells us that, for every value of κ, there will be a modulation frequency which will be equal to a multiple of the nonlinear natural frequency of the system. When this occurs, the system is in resonance. However, the size of these resonances is very sensitive to system parameters ε and κ. In some cases the resonances are infinitely small, while in others they form stable islands. Our simulations predict the formation of large stable resonances for driving amplitudes in the range $\kappa = 0.2$–0.65. Several different methods can be employed to control the velocity

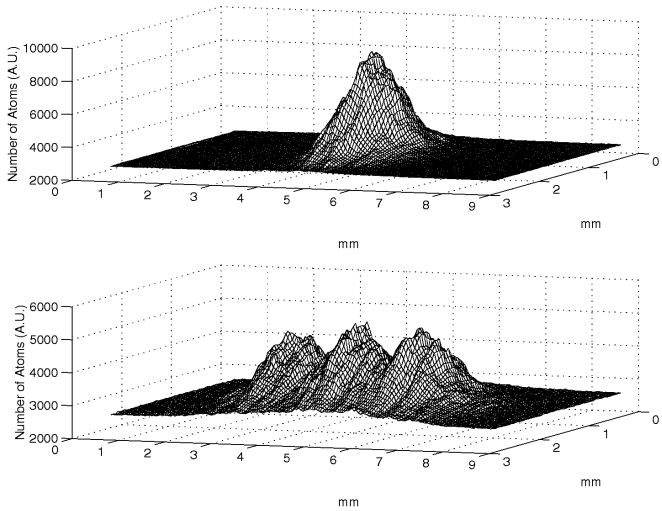

Figure 4. Spatial distributions of the atoms obtained after a 10 ms ballistic expansion interval. The upper distribution results when no interaction potential is applied. The lower distribution shows the resonant structure that results when the atoms interact with 7.5 cycles of a $\omega_m/2\pi = 500$ kHz, $\varepsilon = 0.13$ modulated standing wave.

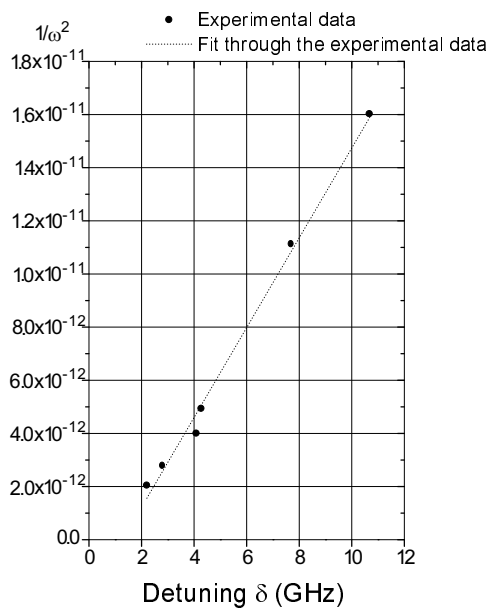

Figure 5. Optimum conditions for observation of phase space resonances. Maximum size of the resonances in the atomic momentum distributions only occurs for certain values of the modulation frequency ω and the detuning δ. The graph shows that maximum size of the resonances occurs for one value of the scaled driving amplitude κ which is proportional to the slope of the graph. (For these results the modulation amplitude ϵ and the light intensity I were kept constant.)

of the resonances. We give a detailed description of the methods in [12]. To roughly adjust the velocity it is most convenient to vary the modulation frequency. As the velocity of the resonant atoms within the wells varies cyclically, fine tuning of the velocity at which they are projected can be achieved by varying the end phase of the standing wave modulation. Furthermore it is possible to vary the velocity slightly by varying the driving amplitude κ and the modulation parameter ϵ. The disadvantage of varying ϵ and κ is that the size of the resonance (width and height) can change drastically. Therefore changing the modulation frequency and the modulation endphase are the most convenient means for velocity control.

We have found that phase space resonances can be observed if the modulated standing wave is turned on for longer than 4.5 cycles. Thereafter, the resonances appear to be stable for many cycles. Figure 6 shows the development of the resonances as a function of the number of modulation periods the standing wave is turned on. These data were taken for an intermediate value of $\bar{k}$ with a modulation frequency $\omega_m/(2\pi) = 500$ kHz and the modulation parameter $\epsilon = 0.13$. One can see that the resonances start to emerge at 4.5 cycles and then remain stable. Figure 9 illustrates that the resonances persist for hundreds of modulation periods, as predicted by theory.

4.2. Transient dynamics

In our discussion of dynamical resonances it is important to avoid confusion with some important transient dynamics which are exhibited by the QDP using a similar experimental setup. These can be used as a coherent atomic beam splitter [25]. Unlike most beam splitters this beam splitter operates outside the Raman–Nath regime because the transverse motion of the atom during its passage through the standing wave is not negligible. Figure 7 shows a typical momentum distribution which results from transient dynamics of the system. Two distinct peaks contain up to 60% of all atoms. This particular picture was taken at a modulation frequency $\omega_m/(2\pi) = 360$ kHz and a modulation parameter $\epsilon = 0.30$. While phase space resonances need at least 4.5 cycles to load sufficiently, the transients occur after only 1.75 modulation periods (cycles) (with a Hamiltonian of the form $I_0(1 + 2\varepsilon \sin \omega_m t)$). The dynamics can be explained classically by following the trajectories of atoms initially equally spaced inside a potential well. A significant number of atoms have climbed to the maximum of the potential well after one cycle. While the potential starts rising again, the atoms 'surf' down the well for the final 0.75 cycles of

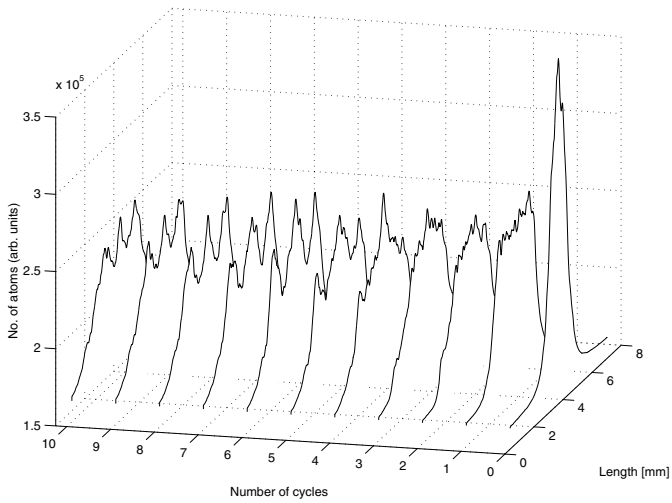

Figure 6. Phase space resonances as a function of the number of modulation periods applied to the initial atomic distribution. Resonances start to emerge at 4.5 cycles. These data were obtained at a modulation frequency of $\omega_m/2\pi = 500$ kHz and a modulation amplitude of $\varepsilon = 0.13$. The resonances move with around 22 recoil momenta.

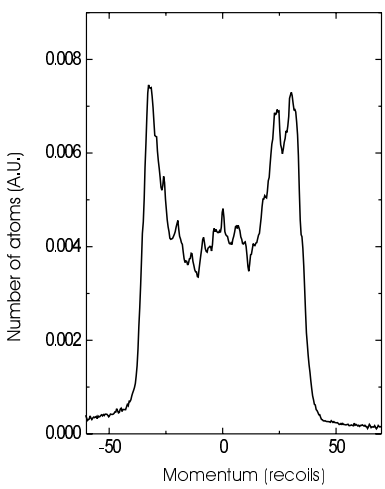

Figure 7. Atomic momentum distribution resulting from the chaotic transients of the system. The momentum peaks have a velocity of 33 recoils and the data were obtained at a modulation frequency of $\omega_m/2\pi = 360$ kHz, a modulation amplitude of $\varepsilon = 0.30$ and after 1.75 cycles of the modulation.

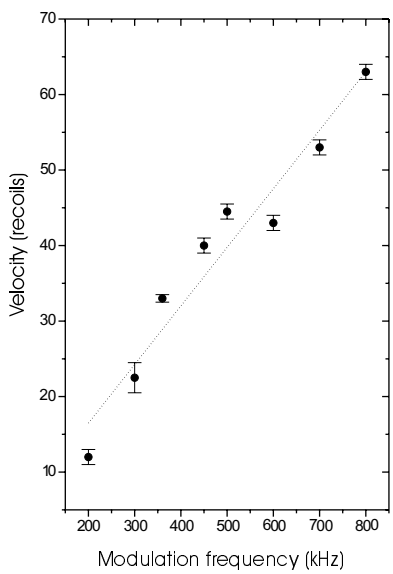

Figure 8. Control of the velocity of the chaotic transients using the modulation frequency. Momenta between 10 and 70 recoils can be achieved. The velocity is approximately a linear function with respect to the modulation frequency.

the modulation. Solving Hamilton's equations one can see that these atoms form a narrow velocity band, which can be observed in the final atomic momentum distribution. As can be seen from figure 7 these peaks have only a small velocity spread, making them a good means to accelerate atoms to some desired velocity. We have observed the transients only for certain values of the light intensity, detuning and modulation frequency. An approximate condition is given by

$$\sqrt{\frac{I}{\delta}} = \varsigma \cdot \omega_m \tag{6}$$

where I is the light intensity, δ is the detuning of the standing wave, ω_m is the modulation frequency and ς is an atom-specific constant.

The velocity of the transient peaks is a function of the modulation frequency. One can easily vary the momentum from 12 to over 60 recoil momenta by adjusting the modulation frequency (and detuning). Figure 8 shows the momentum of the transient peaks as a function of the modulation frequency. A significant momentum range can be covered by changing the modulation frequency. The velocity is approximately a linear function with respect to the modulation frequency. A full discussion of the experimental results can be found in [25]. A different way to use a modulated potential to split an atomic wavefunction coherently was illustrated by Dalibard *et al* [26, 27].

5. On the way to quantum tunnelling and decoherence: loading one resonance effectively

To test predictions of quantum chaos and decoherence it is important to investigate specifically quantum behaviour

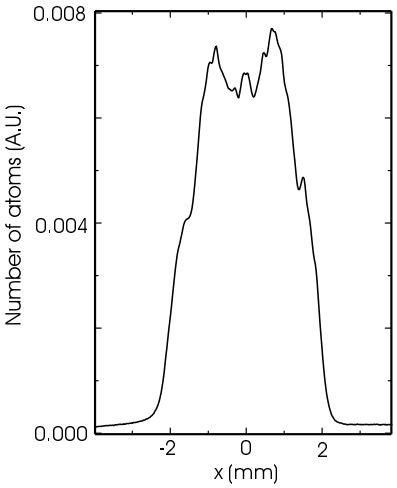

Figure 9. First step to quantum phase space tunnelling. Resonances after an interaction time of 100 periods of the modulation frequency.

of the system. For large values of the scaled Planck's constant $\bar{k}$ quantum effects should become more visible as the size of the atomic wavepackets becomes comparable to the area of the phase space resonances. Quantum tunnelling between two resonances will be an important tool in studying quantum chaos and decoherence. Atoms are predicted to tunnel coherently between the two resonances. The unitary evolution operator, the Floquet operator F, describes the evolution of the QDP in terms of the Floquet eigenstates. These eigenstates are associated with fixed points in the Poincaré section. If we start with a superposition state of two Floquet states which is localized in one resonance, time evolution leads to periodical localization in the other phase space resonance. To observe this quantum tunnelling it is important to prepare atoms in a superposition of Floquet states localized in one resonance. Several methods to achieve this goal are under study.

The observation of resonances for a minimum length of interaction time with the modulation potential is a prerequisite to observe quantum phase space tunnelling, as it is necessary to observe at least a significant part of the tunnelling period to have sufficient evidence for the tunnelling to occur. Tunnelling periods strongly depend on different system parameters. Theoretical calculations have shown that 100 cycles of the modulation frequency are sufficient to observe tunnelling. We have recently observed resonances for an interaction time of 100 periods of the modulation frequency which is an important step towards observation of tunnelling. Figure 9 shows a picture of the resonances after 100 periods of the modulation frequency.

To observe resonances, the starting phase of the standing wave modulation is chosen in such a way that the resonances are located on the position axis of the Poincaré section (atom groups 1 and 2 have zero velocity, see figure 3). In this way both resonances are always loaded. To load only one resonance, atoms can be prepared with a mean momentum equivalent to the resonance velocity relative to the standing wave. The starting phase of the resonance would then be adjusted in such a way that the resonances are located on the momentum axis. If the width of the initial distribution is small enough, only one of the resonances will be loaded.

There are several ways to prepare the atomic cloud with a certain velocity relative to the inertial frame of the standing wave. One possibility is to give the standing wave a constant velocity. This could be achieved by detuning the retroreflecting beam. The velocity of the standing wave c_{st} is given in terms of the detuning by the following condition:

$$c_{\mathrm{st}} = \frac{\omega_1 - \omega_2}{2k} \tag{7}$$

where k is the wavenumber and ω_1 and ω_2 are the frequencies of the two counterpropagating beams. In our case we would need $\omega_1 - \omega_2 \approx 100$ kHz, which could be achieved by utilizing an AOM in each counterpropagating beam and detuning them relative to each other by 100 kHz. The detuning (and therefore the velocity of the standing wave) could be adjusted using an AOM synthesizer driver.

An alternative method to accelerate the atoms is to include an AOM in double-pass configuration in one of the arms of the standing wave. Ramping the frequency difference of the two beams produces an accelerating standing wave. This has been used by Raizen *et al* to demonstrate a Wannier–Stark ladder [3].

Preliminary simulations indicate that, by using the methods introduced above, we may need atoms colder than we currently have as, at the temperatures that we attain, some atoms are still loaded into the other resonance originating from the tail of the atomic Gaussian distribution. To prevent this, a velocity-selective Raman process might be required [28]. After populating the ground state of the potential wells by adiabatically turning on the standing wave [29], the atoms could be prepared in a spatial region of the well corresponding to one of the resonances by means of a controlled phase shift of the optical standing wave.

6. Conclusion

We have shown that atoms in an amplitude-modulated standing wave have some significant properties. Phase space resonances and chaotic transients provide new ways to manipulate atoms. We have explained distinct peaks in the atomic momentum distribution and we showed how to obtain these peaks experimentally. We have investigated the modulation frequency dependence of the velocity of chaotic transients. This provides new means for experiments in atom optics, especially for phase space state preparation. Applications to the study of quantum chaos and decoherence are clear and we have shown pathways to utilize phase space resonances for this. In this study we have shown that the observation of quantum tunnelling should be possible because we were able to observe distinct resonances for 100 periods of the modulation frequency. Further investigations are underway to confirm the predictions of quantum tunnelling for this system. Once quantum tunnelling has been demonstrated it can be used to test predictions of quantum chaos and decoherence. It is easy to vary the scaled Planck's constant as well as the amount of decoherence. This could lead to a better understanding about the connection of quantum mechanics and classical physics. Preparations to see quantum tunnelling are well underway and the first observation is expected to occur shortly.

Acknowledgments

This work is supported by the Australian Research Council. We would like to thank Mark Raizen for suggesting a velocity-selective Raman process to load one of the resonances. We would also like to thank Matthius Hug and Gerard Milburn for valuable discussions about loading one of the resonances.

References

[1] Adams C S, Sigel M and Mlynek J 1994 Atom optics *Phys. Rep.* **240** 143–210
[2] Anderson B P and Kasevich M A 1998 Macroscopic quantum interference from atomic tunnel arrays *Science* **283** 1686–9
[3] Wilkinson S R, Bharucha C F, Madison K W, Niu Q and Raizen M G 1996 Observation of atomic Wannier–Stark ladders in an accelerating optical potential *Phys. Rev. Lett.* **76** 4512–15
[4] McClelland J J, Scholten R E, Palm E C and Celotta R J 1993 Laser-focused atomic deposition *Science* **262** 877–80
[5] Berry M V 1987 Quantum chaology *Proc. R. Soc.* A **413** 183–98
[6] Nakamura K 1997 *Quantum Versus Chaos, Questions Emerging from Mesoscopic Cosmos* (Dordrecht: Kluwer)
[7] Graham R, Schlautmann M and Zoller P 1992 Dynamical localization of atomic-beam deflection by a modulated standing light wave *Phys. Rev.* A **45** R19–22
[8] Moore F L, Robinson J C, Bharucha C F, Bala Sundaram and Raizen M G 1995 Atom optics realization of the quantum δ-kicked rotor *Phys. Rev. Lett.* **75** 4598–601
[9] Ammann H, Gray R, Shvarchuck I and Christensen N 1998 Quantum delta-kicked rotor: experimental observation of decoherence *Phys. Rev. Lett.* **80** 4111–15
[10] Moore F L, Robinson J C, Bharucha C, Williams P E and Raizen M G 1994 Observation of dynamical localization in atomic momentum transfer: a new testing ground for quantum chaos *Phys. Rev. Lett.* **73** 2974
[11] Klappauf B G, Oskay W H, Steck D A and Raizen M G 1998 Observation of noise and dissipation effects on dynamical localization *Phys. Rev. Lett.* **81** 1203–6
[12] Hensinger W K, Truscott A G, Upcroft B, Hug M, Wiseman H M, Heckenberg N R and Rubinsztein-Dunlop H The quantum driven pendulum and its classical analogue in atom optics: an experimental study *Phys. Rev.* A submitted
[13] Arnold V I 1979 *Mathematical Methods of Classical Mechanics* (New York: Springer)
[14] Hug M and Milburn G J Quantum slow motion *Phys. Rev.* A submitted
[15] Dyrting S, Milburn G J and Holmes C A 1993 Nonlinear quantum dynamics at a classical second order resonance *Phys. Rev.* E **48** 969–78
[16] Sanders B C and Milburn G J 1989 The effect of measurement on the quantum features of a chaotic system *Z. Phys. B: Condens. Matter* **77** 497–510
[17] Raab E, Prentiss M, Cable A, Chu S and Pritchard D 1987 Trapping of neutral sodium atoms with radiation pressure *Phys. Rev. Lett.* **59** 2631–4
[18] Dupont-Roc J, Haroche S and Cohen-Tannoudji C 1969 Detection of very weak magnetic fields (10^{-9} Gauss) by ^{87}Rb zero-field level crossing resonances *Phys. Lett.* A **28** 638
[19] Truscott A G, Baleva D, Heckenberg N R and Rubinsztein-Dunlop H 1998 Short-term diffusion in $\sigma^+ - \sigma^-$ optical molasses *Opt. Commun.* **145** 81–5
[20] Chen W, Dyrting S and Milburn G J 1996 Nonlinear dynamics in atom optics *Aust. J. Phys.* **49** 777–818
[21] Charmichael H J 1993 *An Open Systems Approach to Quantum Optics* (Berlin: Springer)
[22] Dyrting S and Milburn G J 1995 Dissipative nonlinear quantum dynamics in atom optics *Phys. Rev.* A **51** 3136–47
[23] Dum R, Zoller P and Ritch H 1992 Monte Carlo simulation of atomic master equation for spontaneous emission *Phys. Rev.* A **45** 4879
[24] Mølmer K, Castin Y and Dalibard J 1993 Monte Carlo wavefunction method in quantum optics *J. Opt. Soc. Am.* B **10** 524
[25] Truscott A G, Friese M E J, Hensinger W K, Wiseman H M, Rubinsztein-Dunlop H and Heckenberg N R 2000 Coherent atomic beam splitter using transients of a chaotic system *Phys. Rev. Lett.* **84** 4023–6
[26] Steane A, Szriftgiser P, Desbiolles P and Dalibard J 1995 Phase modulation of atomic de Broglie waves *Phys. Rev. Lett.* **74** 4972–5
[27] Szriftgiser P, Guéry-Odelin D, Arndt M and Dalibard J 1996 Atomic wave diffraction and interference using temporal slits *Phys. Rev. Lett.* **77** 4–7
[28] Kasevich M, Weiss D S, Riis E, Moler K, Kasapi S and Chu S 1991 Atomic velocimetry selection using stimulated Raman transitions *Phys. Rev. Lett.* **66** 2297–300
[29] Kastberg A, Phillips W D, Rolston S L and Spreeuw R J C 1995 Adiabatic cooling of cesium to 700 nK in an optical lattice *Phys. Rev. Lett.* **74** 1542–5